Raman-assisted phase sensitive amplifier using fiber Bragg grating based tunable phase shifter

YINWEN CAO,[1,*] HAOQIAN SONG,[1] YOUICHI AKASAKA,[2] PEICHENG LIAO,[1] AHMED ALMAIMAN,[1] FATEMEH ALISHAHI,[1] AHMAD FALLAHPOUR,[1] CHANGJING BAO,[1] AMIRHOSSEIN MOHAJERIN-ARIAEI,[1] TADASHI IKEUCHI,[2] DMITRY STARODUBOV,[1] JOSEPH TOUCH,[3] MOSHE TUR,[4] AND ALAN E. WILLNER[1]

[1] *Department of Electrical Engineering, University of Southern California, Los Angeles, CA 90089, USA*
[2] *Fujitsu Laboratories of America, 2801 Telecom Parkway, Richardson, TX 75082, USA*
[3] *Independent consultant, Manhattan Beach, CA 90266, USA*
[4] *School of Electrical Engineering, Tel Aviv University, Ramat Aviv 69978, Israel*
**Corresponding author: yinwenca@usc.edu*

Received XX Month XXXX; revised XX Month, XXXX; accepted XX Month XXXX; posted XX Month XXXX (Doc. ID XXXXX); published XX Month XXXX

A low-loss Raman-assisted phase sensitive amplifier (PSA) with ~20 dB signal net gain is experimentally demonstrated. The amplitude and phase adjustment for PSA is achieved by using non-uniform Raman gain and a tunable fiber Bragg grating (FBG), respectively. The total component loss of the system is measured to be ~8 dB. By tuning the FBG central wavelength, (1) an up-to-5.6 dB signal gain improvement is obtained; and (2) a ~4 dB receiver sensitivity enhancement is observed for 20 and 25 Gbaud QPSK signals and a 10 Gbaud 16-QAM signal.

OCIS codes: *(060.2360) Fiber optics links and subsystems; (060.3735) Fiber Bragg gratings; (060.4370) Nonlinear optics, fibers.*

http://dx.doi.org/10.1364/OL.99.099999

Next generation of enhanced-capacity optical communication systems employing higher-order quadrature amplitude modulation (QAM) have received much attention [1]. These advanced modulation formats can typically benefit from the use of low-noise optical amplifiers to support long-haul transmission. Indeed, the phase sensitive amplifier (PSA) is a potential candidate because it can achieve a lower noise figure than conventional phase insensitive amplifiers [2-5].

PSA relies on a four-wave-mixing (FWM) based parametric nonlinear interaction between a signal, a pump and a so-called idler (copier). By tuning the relative phase between these three components, the correlated signal and idler will undergo constructive coherent addition; concurrently, the uncorrelated noises on the signal and idler will undergo incoherent addition, which results in low-noise amplification. To date, this copier-PSA scheme has been experimentally demonstrated in a variety of different configurations [6-10].

The copier-PSA system typically requires the signal and idler are of similar amplitude, and the phase is matched between the signal, the idler, and the pump. The amplitude and phase adjustment is often achieved by a liquid crystal-on-silicon (LCoS) based programmable filter [6-10], which normally has an insertion loss of ~5 dB [11,12]. This high insertion loss attenuates the power of the signal, the idler and the pump, which decreases the signal net gain (counting the idler generation). Therefore, it might be valuable to have a low-loss copier-PSA system that would provide a high signal net gain.

In this paper, we demonstrate a low-loss Raman-assisted PSA using a fiber Bragg grating (FBG) as a tunable phase shifter to provide ~20 dB signal net gain. Instead of using an LCoS programmable filter, the amplitude and phase adjustment is realized by non-uniform distributed Raman amplification and a tunable low-loss FBG (0.4 dB insertion loss), respectively [13]. The total component loss of the proposed copier-PSA system is measured to be ~8 dB. Compared to a Raman-assisted PSA using a programmable filter with 6.5 dB insertion loss (total component loss is ~14 dB), the proposed approach improves the signal gain by >20 dB because of a reduced link loss for the signal and the PSA pump. Moreover, compared to a system with the FBG of a fixed central wavelength, by tuning the FBG central wavelength, (1) an up-to-5.6 dB signal gain improvement is obtained; and (2) a ~4 dB receiver sensitivity enhancement is demonstrated for 20 and 25 Gbaud QPSK signals as well as a 10 Gbaud 16-QAM signal.

The concept of the proposed Raman-assisted PSA using FBG-based tunable phase shifter is depicted in Fig. 1. This system comprises four stages: (1) idler generation, (2) phase adjustment, (3) hybrid Raman/PSA, and (4) pure PSA. In the stage of idler generation, the PSA pump power is set comparatively low to avoid a significant phase insensitive amplification for the signal itself. Then, a phase adjustment is realized by (1) placing the PSA pump

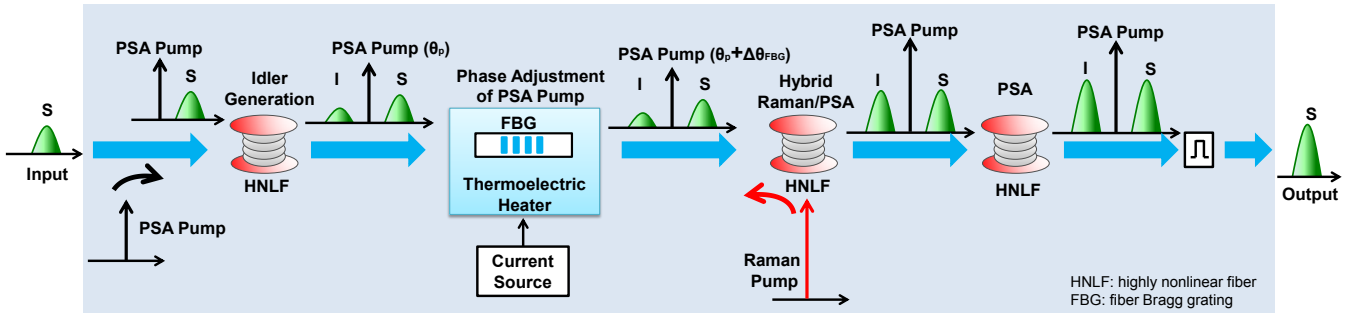

Fig. 1. A schematic diagram of a Raman-assisted PSA using a FBG-based tunable phase shifter. The system includes four stages: (1) idler generation, (2) phase adjustment, (3) hybrid Raman/PSA, and (4) pure PSA. Phase adjustment of the PSA pump is achieved by tuning the central wavelength of the FBG using a thermoelectric heater. Raman amplification is used to boost the power of the PSA pump and compensate for the power imbalance between the signal and idler, by placing the signal away from the effective Raman gain region.

wavelength close to FBG central wavelength; and (2) tuning the FBG central wavelength by varying the FBG temperature, which adds temperature-dependent phase-shift to the pump [14]. Regarding the FBG with a narrow bandwidth (<1 nm), tuning the FBG central wavelength should not affect the signal (S) and idler (I) phase. In the stage of hybrid Raman/PSA, the power imbalance between the signal and idler is compensated by the higher boosting on the idler than the signal, which is achieved by placing the signal wavelength away from the effective Raman gain region. Meanwhile, the PSA pump is also boosted in-line by Raman amplification to enhance the signal gain [15]. Finally, another stage of pure PSA is cascaded for a further signal amplification.

The experimental setup is shown in Fig. 2(a). At the transmitter, a laser is modulated by an optical I/Q modulator driven by an RF signal (QPSK or 16-QAM). The signal input power is adjusted by an attenuator (ATT-1). Meanwhile, a PSA pump at 1566.8 nm is amplified and combined with the signal through a 50/50 coupler. The PSA pump is phase modulated by an 800 MHz pseudo-random binary sequence (PRBS) to suppress stimulated Brillouin scattering (SBS). An optical circulator is used before HNLF-1 to monitor the potential pump power reflection by the FBG during tuning the central wavelength.

An idler is generated with ~−10 dB conversion efficiency in the first stage, in which the signal and the PSA pump (21 dBm) are mixed in a 200 m highly nonlinear fiber (HNLF-1). The nonlinear coefficient, zero dispersion wavelength, and dispersion slope of HNLF-1 are 21.4/W/km, 1551.5 nm, and 0.043 ps/km/nm^2, respectively (The other two HNLFs in the following stages have similar parameters). The input and output spectra of the first stage are shown in Fig. 2(d1–d2), in which the signal is barely amplified.

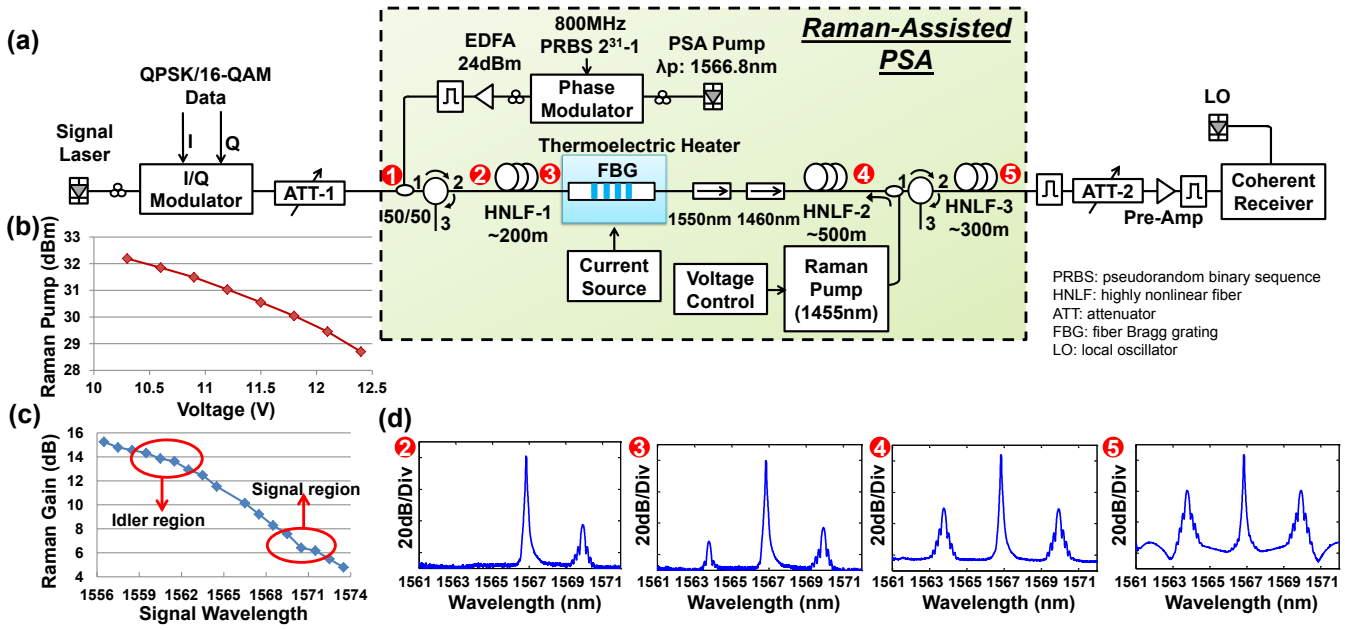

Fig. 2. (a) Experimental setup for a Raman-assisted PSA using a FBG-based tunable phase shifter. The link loss from Node-1 to Node-5 (including the 50/50 coupler, idler generation, phase adjustment, hybrid Raman/PSA, and pure PSA) is ~8 dB. The signal net gain is measured by comparing the signal power between Node-1 and Node-5; (b) Raman pump power vs. control voltage; (c) Raman gain profile, where the idler has more gain than the signal. This helps to decrease the power imbalance between the signal and the idler after idler generation; (d) Spectra at different positions.

In the next stage, the PSA pump, the signal and the idler are sent through a 15-mm-long FBG with a 0.4 dB insertion loss and maximum reflectivity >99%. The FBG is placed on a thermoelectric heater, the surface temperature of which is controlled by a current source. By changing the temperature, the FBG central wavelength moves, adding a phase-shift to the PSA pump. For example, a 0.8 A current increases the FBG temperature by 60°C above room temperature (25 °C) and moves the FBG wavelength by 0.66 nm.

In the third stage, the signal, the idler and the PSA pump are amplified in a 500 m HNLF (HNLF-2) with backward Raman amplification provided by a ~32 dBm Raman pump at 1455 nm. The relationship between Raman pump power and control voltage is shown in Fig. 2(b). The 1460 nm isolator is used to block the output Raman pump; while the 1550 nm isolator is employed to block the potential unwanted SBS. By choosing a signal wavelength longer than 1568 nm (at the edge of the Raman gain region), the signal obtains much less gain from Raman amplification than the idler, as shown in Fig. 2(c). The gain difference between the signal and idler helps to compensate for the power imbalance coming from the first stage (idler generation). Meanwhile, the PSA pump is also boosted by Raman amplification. The spectrum after the hybrid Raman/PSA stage is shown in Fig. 2(d3).

The final stage is a pure PSA process, in which the signal, the pump and the idler are sent to a 300 m HNLF (HNLF-3), where the signal receives additional gain, as shown in Fig. 2(d4).

After HNLF-3, the signal is selected and sent through another attenuator (ATT-2) to adjust the input power for the pre-amplifier before the coherent receiver. ATT-2 is used to fix the input power to the pre-amplifier after each system adjustment/tuning, such as changing Raman pump power, or varying the input signal power.

The relationship between current supply, temperature, and the FBG central wavelength is illustrated in Fig. 3(a). With increasing the injected current, the FBG temperature climbs and its central wavelength is red-shifted. Fig. 3(b) shows that the FBG central wavelength is tuned by changing the temperature and a 60°C temperature increase moves the FBG central wavelength by 0.66 nm. Fig. 3(c) characterizes the phase-shift induced by the thermal

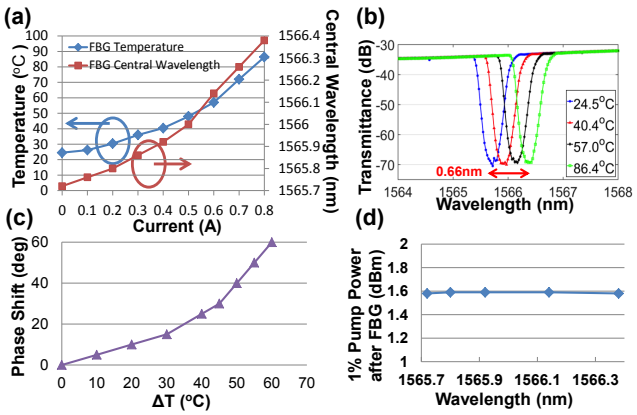

Fig. 3. (a) The current of the thermoelectric heater vs. temperature and FBG central wavelength; (b) FBG transmittance under different temperature levels, in which a 60°C temperature increase shifts the central wavelength by 0.66 nm; (c) Temperature change (ΔT) vs. phase-shift of FBG; (d) 1% PSA pump power after the FBG. The flat curve indicates the PSA pump power is maintained across different FBG central wavelengths.

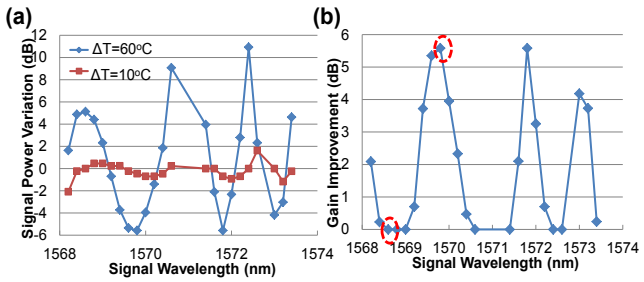

Fig. 4. (a) The variation of output signal power vs. signal wavelength with different FBG temperature changes; (b) Gain improvement by tuning the FBG central wavelength for the signal at different wavelengths.

tuning of the FBG. A temperature change (ΔT) of 30°C provides a phase-shift of ~15 degree while a ΔT of 60°C introduces a phase-shift of ~60 degree. The PSA pump power after the FBG with different central wavelengths is shown is Fig. 3(d). The flat curve indicates the PSA pump power is not significantly decreased by reflection within the wavelength tuning range of 0.66 nm.

Tuning the FBG central wavelength could affect the phase matching condition of the PSA, which is represented by the output power variation of the signal, as shown in Fig. 4(a). It can be seen that a 10°C temperature change, corresponding to a ~5 degree phase-shift for the PSA pump, causes no more than a 2 dB power variation for different input signal wavelengths. However, a 60°C temperature change, corresponding to a ~60 degree phase-shift for the PSA pump, produces a >6 dB power variation. For a range of wavelengths, Fig. 4(b) shows the gain improvement that can be achieved by phase tuning within a ~60 degree range via the FBG tuning. Due to the system dispersion, the optimal phase for each wavelength is different and the signal might already have optimized phase condition for some wavelengths at room temperature. For example, no gain improvement is observed at 1568.6 nm. However, the gain improvement could be 5.6 dB when the signal wavelength is 1569.8 nm.

The wavelength-dependent system optimization is further illustrated by comparing the constellations of a 20 Gbaud QPSK signal in Fig. 5. Since the signal gain varies under different system configurations, the signal power is adjusted by ATT-2 to ensure the same input power to the pre-amplifier. Fig. 5(a) shows that for a signal wavelength of 1569.8 nm, the signal error magnitude vector

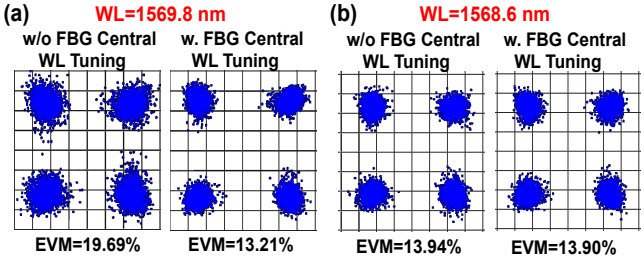

Fig. 5. Comparison of signal constellations between without (w/o) and with (w.) FBG central wavelength tuning. (a) Signal with a wavelength of 1569.8 nm benefits from FBG central wavelength tuning; (b) Signal with a wavelength of 1568.6 nm shows no improvement from FBG central wavelength tuning.

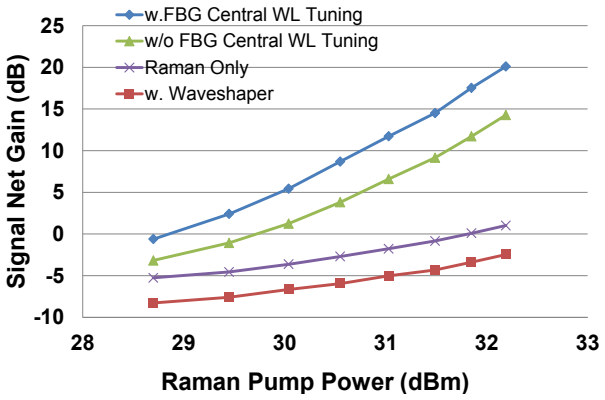

Fig. 6. Comparison of signal net gain (the signal power difference between Node-1 and Node-5 in Fig. 2(a)) under different scenarios: (1) with FBG tuning; (2) without FBG tuning; (3) with Raman amplification only (PSA pump is off); and (4) with waveshaper.

(EVM) is improved by ~6% through tuning the FBG central wavelength. Fig. 5(b) shows that FBG temperature tuning cannot bring extra benefit at a wavelength of 1568.6 nm, because the FBG under the room temperature already provides the optimal phase.

Figure 6 shows the signal net gain (the signal power difference between Node-1 and Node-5 in Fig. 2(a)) by changing the Raman pump power under different scenarios. The signal wavelength is fixed at 1569.8 nm for the remaining part. It can be seen that the system with the FBG central wavelength tuning always provides highest gain under different power levels of the Raman pump. The signal net gain using only Raman amplification is also included, which is <5 dB even the Raman pump power is at its maximum. In addition, the signal net gain is negative if we instead use a programmable filter (waveshaper) with a 6.5 dB insertion loss. This high insertion loss attenuates both the signal and the PSA pump, leading to a significant decrease of the PSA efficiency.

The comparison of bit error rate (BER) performance with and without FBG central wavelength tuning is shown in Fig. 7, including both 20 and 25 Gbaud QPSK signals. It can be seen that FBG central wavelength tuning achieves a similar sensitivity benefit of ~4 dB across the different signal baud rates.

Finally, a 10 Gbaud 16-QAM signal is also demonstrated in the system, as shown in Fig. 8. The benefit of tuning the FBG central wavelength is verified by measuring both EVM and BER. Fig. 8(a) shows that the EVM of the 16-QAM signal is improved by ~2%

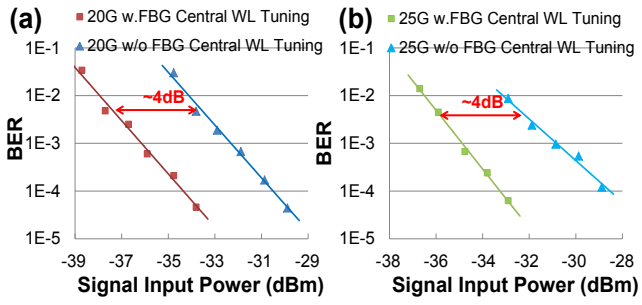

Fig. 7. Comparison of measured BER vs. input power for 20 and 25 Gbaud QPSK signals under two scenarios: (1) without FBG central wavelength tuning; (2) with FBG central wavelength tuning.

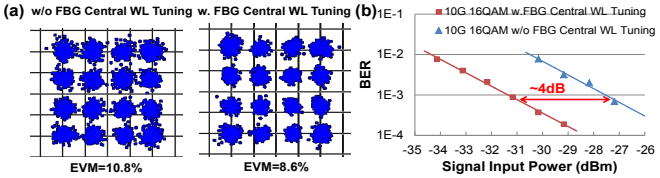

Fig. 8. Comparison of (a) constellation and (b) BER of a 10 Gbaud 16-QAM signal with and without FBG central wavelength tuning.

through tuning FBG central wavelength. This EVM improvement leads to a ~4 dB receiver sensitivity enhancement in Fig. 8(b).

In conclusion, a Raman-assisted PSA with FBG for phase tuning is experimentally demonstrated. The system benefits from the low-loss of the FBG and improves the signal net gain by >20 dB as compared to a system with a programmable filter (waveshaper). A ~4 dB receiver sensitivity enhancement is observed by comparing the systems with and without tuning the FBG central wavelength. It is noted that the current experimental configuration shows a wavelength-dependent signal performance in Fig. 4 and Fig. 5. This phenomenon might be caused by the system dispersion from the discrepancy between zero dispersion wavelength of the HNLFs (~1551 nm) and the PSA pump wavelength (~1567 nm), whose location is determined by the characteristic of the FBG. In future, HNLFs with zero dispersion wavelength close to 1567 nm might enable the extension of the scheme to multi-channel PSA operation.

Funding. Center for Integrated Access Networks (CIAN) (Y501119); Fujitsu Laboratories of America; National Science Foundation (NSF) (ECCS-1202575)

Acknowledgment. We thank Furukawa Electric Co. LTD for the use of their equipment.

References

1. S. Beppu, K. Kasai, M. Yoshida, and M. Nakazawa, Opt. Exp.**23**, 4960 (2015).
2. C. M. Caves, Phys. Rev. D **26**, 1817(1982).
3. M. Vasilyev, Opt. Exp. **13**, 7563 (2005).
4. Z. Tong, C. Lundstrom, P. A. Andrekson, C. J. McKinstrie, M. Karlsson, D. J. Blessing, E. Tipsuwannakul, B. J. Puttnam, H. Toda, and L. Gruner-Nielsen, Nat. Photon. **5**, 430 (2011).
5. T. Kazama, T. Umeki, M. Abe, K. Enbutsu, Y. Miyamoto, and H. Takenouchi, J. Lightw. Technol. **35**, 755 (2017).
6. A. Albuquerque, B. Puttnam, J. Mendinueta, M. Drummond, S. Shinada, R. Nogueira, and N. Wada, Opt. Lett. **40**, 288 (2015).
7. J. Kakande, C. Lundström, P. A. Andrekson, Z. Tong, M. Karlsson, P. Petropoulos, F. Parmigiani, and D. Richardson, Opt. Exp. **18**, 4130 (2010).
8. K. J. Lee, F. Parmigiani, S. Liu, J. Kakande, P. Petropoulos, K. Gallo, and D. Richardson, Opt. Exp. **17**, 20393 (2009).
9. R. Neo, J. Schröder, Y. Paquot, D-Y Choi, S. Madden, B. Luther-Davies, and B. J. Eggleton, Opt. Exp. **21**, 7926 (2013).
10. Y. Zhang, C. Husko, J. Schröder, S. Lefrancois, I. H. Rey, T. F. Krauss, and B. J. Eggleton, Opt. Lett. **39**, 363 (2014).
11. J. Hou, L. Chen, W. Dong, and X. Zhang, Opt. Exp. **24**, 2701 (2016).
12. H. Zhang, M. Tang, Y. Xie, H. Liao, S. Fu, P. Shum, and D. Liu, Appl. Phys. B **112**, 479 (2013).
13. Y. Cao, H. Song, Y. Akasaka, A. Almaiman, A. Mohajerin-Ariaei, C. Bao, P. Liao, F. Alishahi, A. Fallahpour, T. Ikeuchi, D. Starodubov, J. Touch, and A. E. Willner, Proc. ECOC, W.3.B.2 (2017).
14. S. Y. Li, N. Q. Ngo, S. C. Tjin, P. Shum, and J. Zhang, Opt. Lett. **29**, 29 (2004).
15. X. Fu, X. Guo, and C. Shu, Sci Rep. **6**, 1 (2016).

References (Long Format)

1. S. Beppu, K. Kasai, M. Yoshida, and M. Nakazawa, "2048 QAM (66 Gbit/s) single-carrier coherent optical transmission over 150 km with a potential SE of 15.3 bit/s/Hz," in Optics Express, vol. 23, no. 4, pp. 4960-4969, 2015.
2. C. M. Caves, "Quantum limits on noise in linear amplifiers," in Physical Review D, vol. 26, no. 8, pp. 1817-1839, 1982.
3. M. Vasilyev, "Distributed phase-sensitive amplification," in Optics Express, vol. 13, no. 19, pp. 7563-7571, 2005.
4. Z. Tong, C. Lundstrom, P. A. Andrekson, C. J. McKinstrie, M. Karlsson, D. J. Blessing, E. Tipsuwannakul, B. J. Puttnam, H. Toda, and L. Gruner-Nielsen, "Towards ultrasensitive optical links enabled by low-noise phase-sensitive amplifiers," in Nature Photonics, vol. 5, pp. 430-436, 2011.
5. T. Kazama, T. Umeki, M. Abe, K. Enbutsu, Y. Miyamoto, and H. Takenouchi, "Low-Parametric-Crosstalk Phase-Sensitive Amplifier for Guard-Band-Less DWDM Signal Using PPLN Waveguides," in Journal of Lightwave Technology, vol. 35, no. 4, pp. 755-761, 2017.
6. A. Albuquerque, B. Puttnam, J. Mendinueta, M. Drummond, S. Shinada, R. Nogueira, and N. Wada, "Experimental investigation of phase-sensitive amplification of data signals in a four-mode fiber-based PSA," in Optics Letters, vol. 40, no. 2, pp. 288-291, 2015.
7. J. Kakande, C. Lundström, P. A. Andrekson, Z. Tong, M. Karlsson, P. Petropoulos, F. Parmigiani, and D. Richardson, "Detailed characterization of a fiber-optic parametric amplifier in phase-sensitive and phase-insensitive operation," in Optics Express, vol. 18, no. 5, pp. 4130-4137, 2010.
8. K. J. Lee, F. Parmigiani, S. Liu, J. Kakande, P. Petropoulos, K. Gallo, and D. Richardson, "Phase sensitive amplification based on quadratic cascading in a periodically poled lithium niobate waveguide," in Optics Express, vol. 17, no. 12, pp. 20393-20400, 2009.
9. R. Neo, J. Schröder, Y. Paquot, D-Y Choi, S. Madden, B. Luther-Davies, and B. J. Eggleton, "Phase-sensitive amplification of light in a χ(3) photonic chip using a dispersion engineered chalcogenide ridge waveguide," in Optics Express, vol. 21, no. 7, pp. 7926-7933, 2013.
10. Y. Zhang, C. Husko, J. Schröder, S. Lefrancois, I. H. Rey, T. F. Krauss, and B. J. Eggleton, "Phase-sensitive amplification in silicon photonic crystal waveguides," in Optics Letters, vol. 39, no. 2, pp. 363-366, 2014.
11. J. Hou, L. Chen, W. Dong, and X. Zhang, "40 Gb/s reconfigurable optical logic gates based on FWM in silicon waveguide," in Optics Express, vol. 24, no. 3, pp. 2701-2711, 2016.
12. H. Zhang, M. Tang, Y. Xie, H. Liao, S. Fu, P. Shum, and D. Liu, "Programmable all-fiber structured waveshaper based on linearly chirped fiber Bragg grating and digital thermal controller," in Applied Physics B, vol. 112, no. 4, pp. 479-484, 2013.
13. Y. Cao, H. Song, Y. Akasaka, A. Almaiman, A. Mohajerin-Ariaei, C. Bao, P. Liao, F. Alishahi, A. Fallahpour, T. Ikeuchi, D. Starodubov, J. Touch, and A. E. Willner, "Experimental Investigation on the Effect of Central Wavelength Tuning of FBG-Based Phase Shifter for Raman-Assisted Phase Sensitive Amplifier," in Proc. ECOC, Gothenburg, Sweden, Sep. 17–21, 2017, Paper W.3.B.2.
14. S. Y. Li, N. Q. Ngo, S. C. Tjin, P. Shum, and J. Zhang, "Thermally tunable narrow-bandpass filter based on a linearly chirped fiber Bragg grating," in Optics Letters, vol. 29, no. 1, pp. 29-31, 2004.
15. X. Fu, X. Guo, and C. Shu, "Raman-Enhanced Phase-Sensitive Fibre Optical Parametric Amplifier," in Scientific Report, vol. 6, pp. 1-8, 2016.